

Article

Robust Carbon-Stabilization of Few-Layer Black Phosphorus for Superior Oxygen Evolution Reaction

Mengjie Zhang, Wenchang Zhu, Xingzhe Yang, Meng Feng and Hongbin Feng * 

Institute of Materials for Energy and Environment, School of Materials Science and Engineering, Qingdao University, Qingdao 266071, China; zmjqdu@163.com (M.Z.); wenchangars@163.com (W.Z.); 15705420798@163.com (X.Y.); fengmeng16@163.com (M.F.)

* Correspondence: fenghongbin@qdu.edu.cn

Received: 9 June 2020; Accepted: 17 July 2020; Published: 19 July 2020



Abstract: Few-layer exfoliated black phosphorus (Ex-BP) has attracted tremendous attention owing to its promising applications, including in electrocatalysis. However, it remains a challenge to directly use few-layer Ex-BP as oxygen-involved electrocatalyst because it is quite difficult to restrain structural degradation caused by spontaneous oxidation and keep it stable. Here, a robust carbon-stabilization strategy has been implemented to prepare carbon-coated Ex-BP/N-doped graphene nanosheet (Ex-BP/NGS@C) nanostructures at room temperature, which exhibit superior oxygen evolution reaction (OER) activity under alkaline conditions. Specifically, the as-synthesized Ex-BP/NGS@C hybrid presents a low overpotential of 257 mV at a current density of 10 mA cm⁻² with a small Tafel slope of 52 mV dec⁻¹ and shows high durability after long-term testing.

Keywords: black phosphorus; carbon-coating; oxygen evolution reaction; N-doped graphene

1. Introduction

Energy generation systems in modern industry mainly rely on the burning of fossil fuels, which causes environmental deterioration issues. Therefore, the development of new sustainable electrochemical energy technologies has received wide attention, among which the use of water electrolysis for hydrogen production has attracted much attention due to its efficient and clean energy source nature [1–3]. However, as a half reaction of electrocatalytic water splitting, the sluggish kinetics of the oxygen evolution reaction (OER) has become the most challenging issue that limits the efficiency of these electrochemical systems [4–6]. Electrocatalysts play important roles as key components in OER. Currently, the Ir/Ru-based noble metal catalysts possess the best OER electrocatalytic activity, but the scarcity of these metals on Earth and consequent high-cost severely limit their practical application [7]. Therefore, the development of highly efficient but more cost-effective noble metal-free electrocatalytic OER catalysts is an important research direction in this field.

More recently, two-dimensional (2D) ultrathin materials have considered as a type of ideal catalysts due to their distinctive physical and chemical properties [8–10]. Especially, black phosphorus (BP) is believed as a very promising candidate for OER owing to its remarkable electrical conductivity, large specific surface area, and effective electrocatalytic activity [11–15]. However, the few-layer BP is usually in a thermodynamic metastable state with high surface energy and poor antioxidant capacity in air or dissolved oxygen solutions [16–18]. In many applications, the surface oxidation of BP results in performance degradation due to reduced electrical conductivity and passivation of reaction interfaces. Unfortunately, it is difficult to avoid this undesirable phenomenon during the preparation of few-layer BP or its composites. This limitation has become one of the key obstacles towards the development and application of phosphorene-based materials.

To date, several strategies have been used to protect BP from degradation that depend on avoiding its exposure to atmospheric conditions. Some surface coating processes or functionalization methods such as inorganic or organic covalent functionalization and hybrid organic-inorganic coatings have been used as a physical barrier to prevent oxygen from reaching the surface [19–23]. However, these coating layers may also occupy the active catalytic sites, reducing the conductivity of the materials, which leads to poor applicability of the catalysts. Recently, carbon coating has been used as a protective coating layer for functional materials to enhance their applications [24–26]. Carbon dioxide is a greenhouse gas, but it is also a readily available carbon source. The direct chemical conversion of CO₂ into carbon coating materials is not only a way to convert and store this greenhouse gas, but also a novel method to prepare carbon coatings.

Here, a facile method to produce carbon-coated exfoliated black phosphorus/N-doped graphene nanosheets (Ex-BP/NGS) hybrids was reported using CO₂ as the carbon source at room temperature. Sodium/potassium (NaK) alloy was used as both the CO₂ reducing agent and the intercalating reagent of the bulk BP. The composite material was made by in-situ exfoliation of bulk BP and simultaneous reduction of CO₂. Moreover, the carbon-coated layer derived from CO₂ can enhance the contact between N-doped graphene nanosheets (NGS) and Ex-BP nanosheets which is beneficial to improve the electrochemical stability. Due to the combination of carbon coating layer and NGS protection, the Ex-BP/NGS hybrid presents excellent OER performance.

2. Materials and Methods

2.1. Synthesis of NGS

The N-doped graphene nanosheets (NGS) were synthesized by a quenching process of H₂SO₄-intercalated graphite in a sodium-ammonia solution. The graphite was firstly immersed in oleum for 24 h. Then, most of the acid was removed by filtration, and quickly added into sodium-ammonia solution, which is formed by dissolving 800 mg of sodium in 100 mL of liquid ammonia.

2.2. Synthesis of Ex-BP

Black phosphorus crystals with a purity of 99.998% were purchased from the XFNANO Company (Nanjing, China). Typically, sodium (Na) metal (0.1 g) and potassium (K) metal (0.3 g) were squeezed together in 1,2-dimethoxyethane (DME, 100 mL). As a result, the liquid NaK alloy was formed in an argon-filled glove box. Black phosphorus powder (200 mg) which was obtained by grinding black phosphorus crystals for 10 min in advance were added to DME (150 mL). Then, NaK alloy was added under the protection of argon, and mixed with high-shearing treatment (FA2 high-shear mixer, FLUKO, Shanghai, China) for 30 min. Figure S1a,b showed the equipment for synthesizing Ex-BP/NGS@C and the photos of the synthesis process. The reaction products were separated by centrifugation and washed with ethanol and water five times.

2.3. Synthesis of Ex-BP/NGS

Black phosphorus powder (200 mg) and NGS (200 mg) were added to DME (150 mL). Then, Ex-BP/NGS was successfully prepared through the same reaction conditions and cleaning process as Ex-BP.

2.4. Synthesis of Ex-BP/NGS@C

The preparation of liquid NaK alloy was performed as described above. First, the BP powder (200 mg) and NGS powder (200 mg) were mixed together in DME (150 mL), and then the liquid NaK alloy was added with argon protection. Subsequently, the reaction mixture was treated by high-shearing treatment for 30 min. Then, the CO₂ was added at 80 mL/min for 30 min. The CO₂ was converted into carbon coating layers via the reactions as shown in Figure 1. The final products were

centrifuged and washed with absolute ethyl alcohol and distilled water five times. Figure S1c showed the image of final product Ex-BP/NGS@C dispersed in aqueous solution.

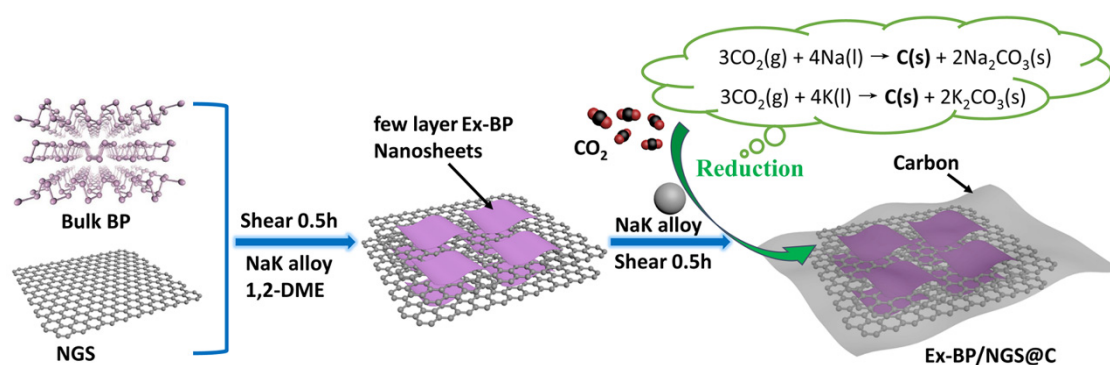


Figure 1. Schematic diagram of the preparation of the Ex-BP/NGS@C hybrid material.

2.5. Product Characterization

XRD measurements were conducted on an Ultima IV X-ray diffractometer (Rigaku, Austin, TX, USA) equipped with Cu K α radiation ($\lambda = 0.15418$ nm). Raman spectra were obtained on an inVia Plus Micro-Raman spectroscopy system (Renishaw, London, England) equipped with a 50 mW DPSS laser at 532 nm. XPS peaks were obtained by an Escalab 250Xi electron spectrometer system (Al K α $h\nu = 1486.6$ eV, Thermo, Waltham, MA, USA). Large beam spot: Ag 3d_{5/2} (FWHM = 0.50 eV) intensity ≥ 400 kcps; 20 μm beam spot: Ag 3d_{5/2} (FWHM = 0.45 eV) intensity ≥ 0.5 kcps. Transmission electron microscopy (TEM, JEM-2100, JEOL, Tokyo, Japan) was used to observe the morphology and crystal structure of the samples. A SPI 4000 system in tapping mode (NSK, Japan) was used to perform AFM measurements. The EDS images were obtained by using a Titan Themis 200 TEM (FEI, Hillsboro, OR, USA) equipped with a super-X EDS system (Bruker, Germany).

2.6. Electrochemical Measurements

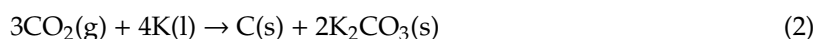
The catalyst inks for electrochemical tests were made by dispersing catalyst (5 mg), carbon black (1 mg), ethanol (1 mL) and Nafion solution (5 wt.%, 15 μL) under sonication for 30 min. The above solution (8 μL) was pipetted through a pipette and transferred onto a freshly polished glassy carbon electrode. After drying the glassy carbon electrode, a working electrode with a uniform distribution of catalyst with a loading of 0.57 mg cm⁻² can be obtained. Electrochemical tests were performed using an electrochemical workstation (CHI660E, Shanghai, China) and a three-electrode system in 1 M KOH electrode solution. An Hg/HgO electrode and a carbon rod were used as reference electrode and counter electrode, respectively. In all electrochemical tests, the electrode potential vs. Hg/HgO were converted to that vs. reversible hydrogen electrode (RHE) according to the Nernst equation ($E(\text{RHE}) = E(\text{Hg}/\text{HgO}) + 0.059 \times \text{pH} + 0.098$). The electrochemical impedance spectroscopy (EIS) measurements were performed on a PGSTAT302N system (Autolab, Switzerland) at a charged state with a 5 mV amplitude.

3. Results and Discussion

The production of the Ex-BP/NGS@C hybrid is schematically illustrated in Figure 1. To enhance the stability of Ex-BP, we introduced both a carbon coating layer and N-doped graphene sheets (NGS) to passivate Ex-BP. The whole process is performed in one-pot at room temperature.

First, the bulk BP powder and NGS powder were mixed together with some sodium/potassium (NaK) alloy by a high-shearing treatment for 0.5 h. Bulk BP crystals were exfoliated into ultrathin nanosheets (Ex-BP) via simple shearing treatment in 1,2-dimethoxyethane (DME). Herein, the NGS was produced by directly chemical exfoliation of graphite in the presence of sodium-ammonia solution (experimental section). The liquid NaK alloy shows some intercalation properties for layered materials

as well as a very strong reducibility [27,28]. As shown in Figure 1, Ex-BP nanosheets were directly exfoliated by the combined contribution of shearing-assistance and the chemical intercalation process. Second, the pure CO₂ was subsequently added into this solution. Then, the amorphous carbon derived from CO₂ reduction was used as the carbon coating. The conversion of CO₂ into amorphous carbon coating was conducted by the following reactions:



As shown in Figure 2, the transmission electron microscopy (TEM) and high-resolution TEM (HRTEM) images illustrated the morphologies of the 2D Ex-BP/NGS@C hybrids. The 2D structure of Ex-BP/NGS@C can be clearly observed in Figure 2a. The interlayer spacing of 0.21 nm corresponds to the (002) lattice plane of Ex-BP nanosheets. As shown in Figure 2b, the HRTEM image with an interlayer spacing of 0.37 nm revealed that the NGS nanosheets contained about five layers. Furthermore, the amorphous carbon that was coated on the Ex-BP nanosheets can be clearly observed in the HRTEM image in Figure 2b. The corresponding fast Fourier transform image shows a dispersion ring that also demonstrates the existence of the amorphous carbon. TEM image of Ex-BP in Figure S2 presents a free-standing nanosheet, which demonstrated the successful exfoliation of the bulk BP. The thickness of Ex-BP is determined to be about ~3.6 nm by atomic force microscopy (AFM) observation (Figure S3) that corresponds to a few layers (5–7 layers) of sheets. The selective-area electron diffraction pattern (SAED) reveals the crystalline performance of Ex-BP nanosheets with [010] preferential orientation [29]. Figure 2e shows the elemental mapping for C, N and P of Ex-BP/NGS@C hybrid (Figure 2c,f). The uniform distribution of all elements clearly indicates that Ex-BP nanosheets have good contact with NGS and amorphous carbon.

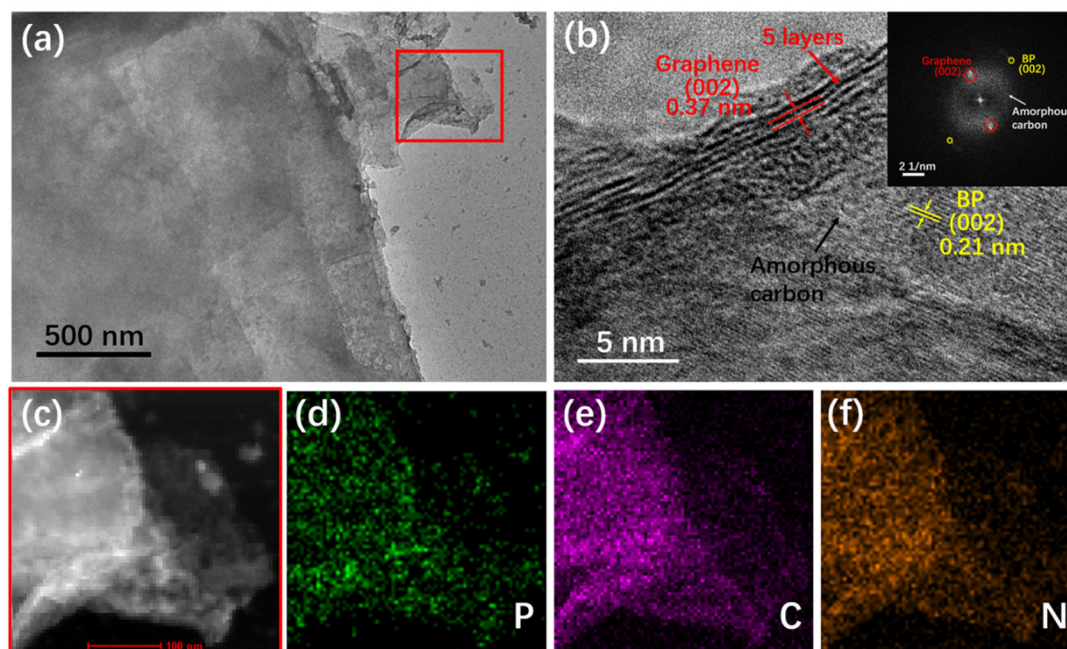


Figure 2. (a) TEM image of Ex-BP/NGS@C. (b) HRTEM image of Ex-BP/NGS@C to the edge location in (a). (c–f) STEM-EDS elemental mapping images of Ex-BP/NGS@C.

Powder X-ray diffraction (XRD) was used to test the crystalline phases of all samples. Figure 3a shows the XRD patterns of bulk BP, NGS, Ex-BP/NGS and Ex-BP/NGS@C, respectively. The main characteristic of high crystalline BP was displayed as three strong intensity of (020), (040) and (060) peaks at 17.0°, 34.2° and 52.4°, respectively [30]. The peak at 26.4° is a characteristic peak of NGS.

Figure 3b shows the Raman spectra of the bulk BP, NGS, Ex-BP/NGS and Ex-BP/NGS@C. The Raman peaks of bulk BP at 362.2, 439.3, and 466.2 cm^{-1} can be assigned to the characteristic Ag1, B2g, and Ag2 vibrational modes, respectively [31]. The Raman spectrum of Ex-BP/NGS and Ex-BP/NGS@C also demonstrates three peaks, indicating that both Ex-BP/NGS and Ex-BP/NGS@C maintain the characteristic vibration structure of bulk BP. The two strong bands centered at 1330 and 1580 cm^{-1} are assigned to the in-plane vibrations of disordered amorphous carbon (D band) and crystalline graphitic carbon (G band), respectively. The chemical states of Ex-BP/NGS@C were analysed by XPS measurements. The survey XPS spectrum of Ex-BP/NGS@C verifies the presence of P, N, C, and O peaks (Figure 3c). Figure 2d shows the high-resolution P 2p spectra of Ex-BP/NGS@C. Three prominent peaks located at 130.5, 131.3 eV are characteristic for P 2p_{3/2} and P 2p_{1/2} [32]. The peaks at 134.8, 135.5 and 136.4 eV are characteristic for oxidized phosphorus (P–O–C, P–O–P and O–P=O) binding energies (BE), respectively [33]. Moreover, the peaks at 133.6 and 284.2 eV corresponding to P–C bond are observed in P 2p and C 1s XPS spectra in Figure 3d,e, which demonstrated that a strong contact is formed between the Ex-BP nanosheets and carbon coating layer [33]. The N 1s XPS spectra in Figure 3f can be indexed to quaternary N, pyrrolic N and pyridinic N in NGS. We also have further conducted an FTIR test on Ex-BP/NGS@C and demonstrated the characteristic peak of P–O and P–C in Figure S4 in the supporting information.

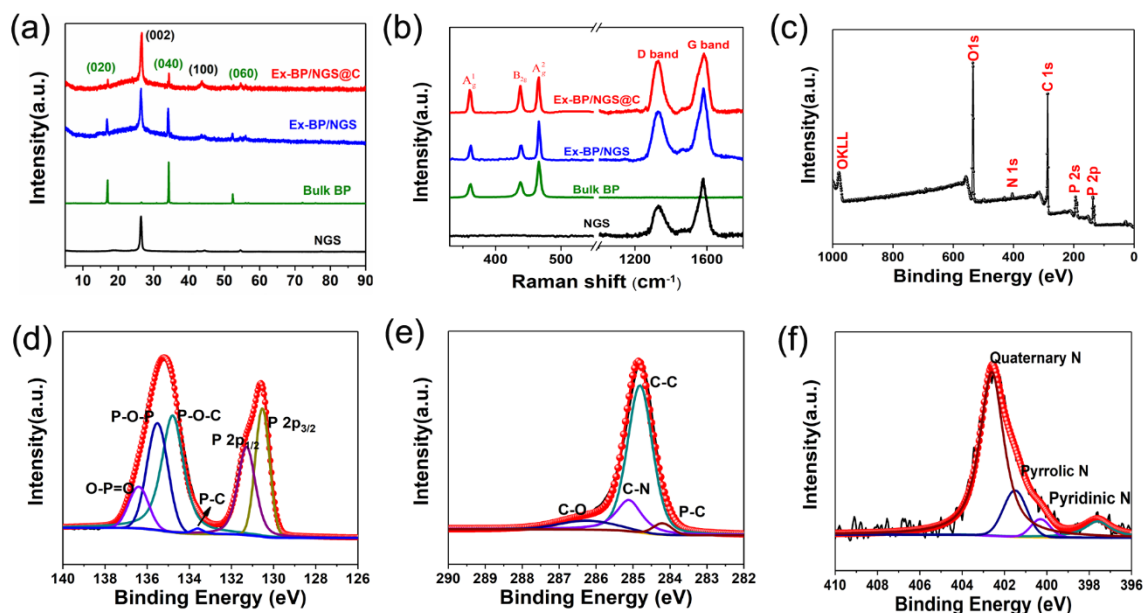


Figure 3. (a) XRD patterns of the Bulk BP, NGS, Ex-BP/NGS@C and Ex-BP/NGS. (b) Raman scattering spectra of the Bulk BP as well as NGS, Ex-BP/NGS@C and Ex-BP/NGS. (c–f) XPS survey and high-resolution XPS spectra of C 1s for Ex-BP/NGS@C.

The obtained Ex-BP/NGS@C hybrid was tested as an electrocatalyst for the oxygen evolution reaction (OER). Figure 4a shows the schematic diagram of the carbon-stabilization strategy by carbon-coated Ex-BP/N-doped graphene nanosheet nanostructures. In order to evaluate the OER activity of Ex-BP/NGS@C, Ex-BP/NGS, bulk BP and NGS, we used a three-electrode system for testing. All tests were performed in 1 M KOH. As shown in Figure 4b, compared with Ex-BP/NGS and Bulk-BP, Ex-BP/NGS@C exhibits the best OER performance. The onset potential of Ex-BP/NGS@C is about 1.43 V vs. RHE, which is higher than the sample without carbon derived CO₂, whose onset potential is 1.53 V vs. RHE. Furthermore, in all the comparative samples Ex-BP/NGS@C shows the largest current density at the same voltage. This may be because the carbon coated on the surface of the sample makes the combination of black phosphorus and NGS more compact, which is beneficial to the electron transfer from the NGS surface to the black phosphorus surface. This phenomenon can also be proved from the

Figure 5a. Ex-BP/NGS@C has a smaller charge transfer resistance ($R_{ct} \approx 63 \Omega$), which is conducive to electron transport. In addition, we tested the oxygen evolution performance of bulk-BP. As can be seen from the linear sweep voltammetry (LSV) curve, bulk-BP has almost no oxygen evolution properties. The layer-to-layer stacking between them results in a smaller surface area, less active site exposure and poorer electron conductivity [34]. The Tafel slope of the material can be fitted from Figure 4c, 52, 54, 67, 90 mV dec^{-1} respectively corresponds to Ex-BP/NGS@C, Ex-BP/NGS, Ex-BP and RuO_2 (99.9% metals basis, Aladdin). The Tafel slope of sample Ex-BP/NGS@C is smaller, corresponding to a higher catalytic activity [35]. More importantly, derived carbon obtained by reducing carbon dioxide not only accelerates the transfer speed of electrons, but also contributes significantly to maintaining the stability of OER performance. Figure 4d,e show the stability of Ex-BP/NGS@C and Ex-BP/NGS. The LSV curves after 2800 cycles of the sample without carbon show its catalytic activity has a significant decline. The Ex-BP/NGS@C maintained a high degree of coincidence with the initial polarization curve after 2800 cycles, which confirmed the excellent stability of all samples we synthesized.

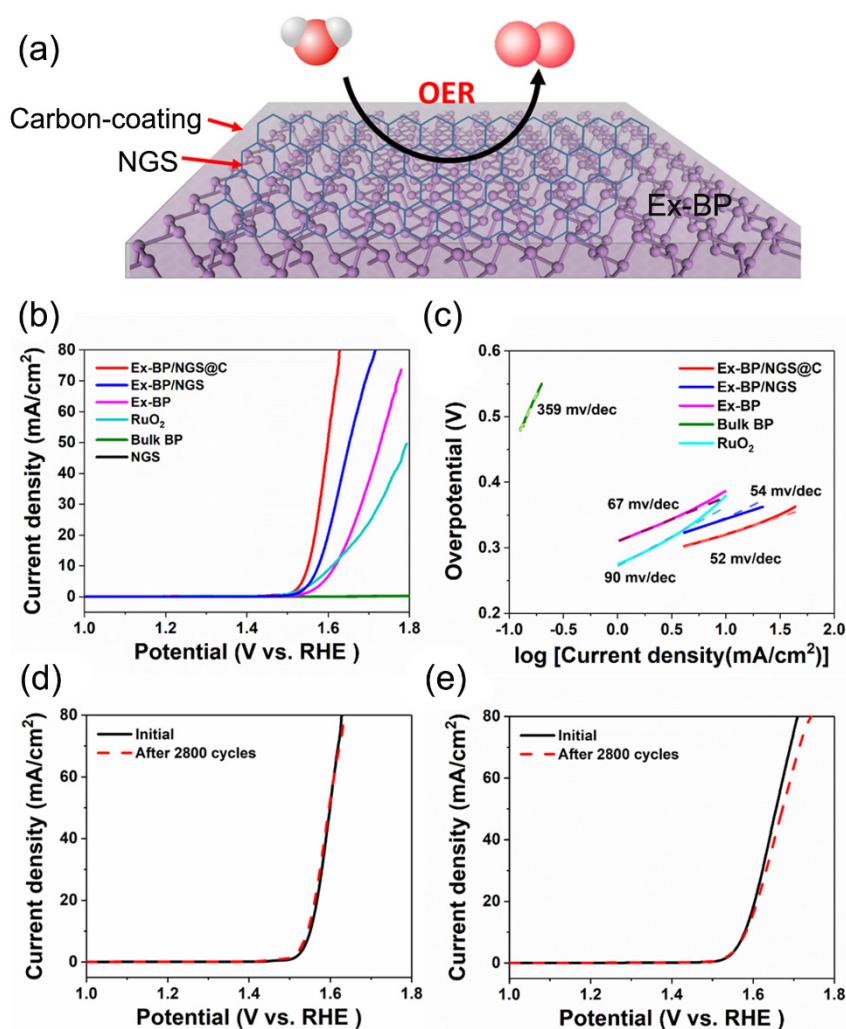


Figure 4. (a) The schematic diagram of the carbon-stabilization strategy, (b) LSV curves, (c) Tafel plots for Ex-BP/NGS@C, Ex-BP/NGS, Ex-BP, Bulk BP and NGS catalysts. Stability test of the (d) Ex-BP/NGS@C and (e) Ex-BP/NGS by CV scanning 2800 cycles with a scan rate of 100 mV/s.

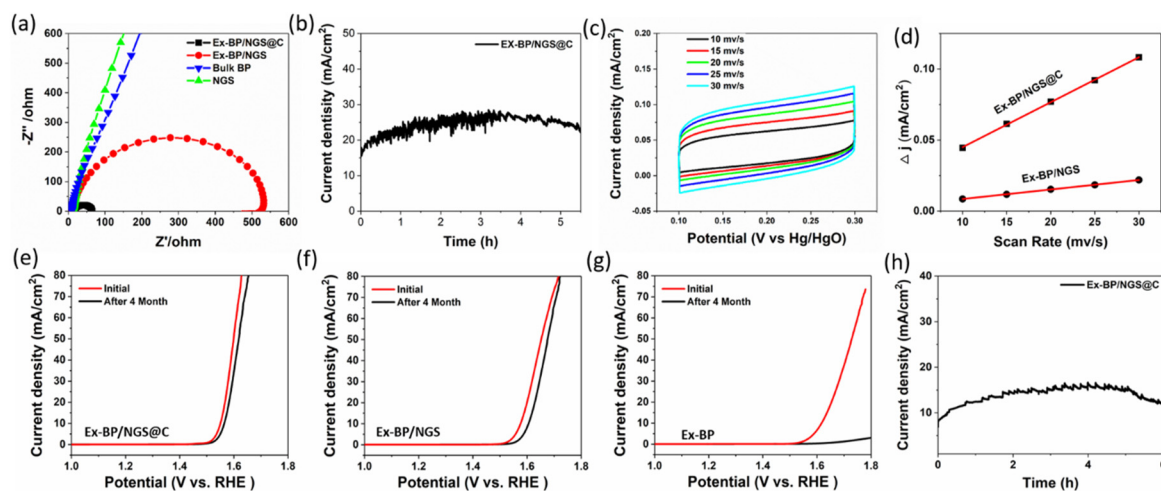


Figure 5. (a) Nyquist plots of EIS for all samples in 1 M KOH electrolyte, (b) $I-t$ curve of Ex-BP/NGS@C in 1 M KOH electrolyte concentration during oxygen evolution process. (c) Cyclic voltammograms at different scan rates of Ex-BP/NGS@C to estimate of electrochemical active surface area (ECSA). (d) Plot of the charging current density differences at 0.20 V vs. the scan rate. Comparison of LSV curves of Ex-BP/NGS@C (e), Ex-BP/NGS (f) and Ex-BP (g) stored under the same storage conditions for 4 months. (h) $I-t$ curve of Ex-BP/NGS@C in 1 M KOH electrolyte concentration during oxygen evolution process after storage 4 months.

The charge transfer resistances (R_{ct}) of all catalysts were assessed to understand the electrode kinetics of the studied catalysts for OER. We use electrochemical impedance spectrum (EIS) to evaluate the electrode kinetic parameters of materials in the electrocatalytic oxygen evolution reaction [14]. Figure 5a shows the EIS Nyquist plots for Ex-BP/NGS@C, Ex-BP/NGS, Ex-BP, Bulk BP and NGS catalysts at the onset potential. It was found that the R_{ct} of the Ex-BP/NGS@C sample (63 Ω) is much smaller than those of other samples such as Ex-BP/NGS (520 Ω). The material with the best catalytic performance has the lowest charge transfer resistance. This indicates highly efficient electron transport and favorable OER kinetics at the Ex-BP/NGS@C electrolyte interface. Figure 5b show the long-term stability of Ex-BP/NGS@C. In the 5.5 h during which the oxygen evolution reaction continues, there is no significant decrease in current density, indicating that it can maintain catalytic activity for a longer period of time at a higher current density. To further unveil the electrochemically active area, the CV curves of Ex-BP/NGS@C at different sweep speeds were tested (Figure 5c). As shown in Figure 5d, Δj is linear growth with sweep speeds; and the slope of the line is twice of the double-layer capacitance [36]. As a result, Ex-BP/NGS@C (3.16 mF cm^{-2}) is larger than the slope of Ex-BP/NGS (0.67 mF cm^{-2}). According to ECSA test comparison results, sample coated with carbon dioxide-derived carbon exhibit greater electrochemically active area, representing an increase in the effective oxygen evolution activity of electrolytic water.

Figure 5e manifests that the oxygen evolution performance Ex-BP/NGS@C undergoes a slight drop after being stored in ethanol for 4 months owing to the double protection of NGS and C. Compared with the sample which only has protection without carbon dioxide derived carbon (Figure 5f) the electrochemical activity is maintained well. Figure 5g shows the oxygen evolution performance of a few-layer black phosphorus sample stripped by the same method. Since black phosphorus is easily oxidized and loses catalytic activity, the performance of the sample after long-term storage is significantly degraded. In the absence of any carbon protection, the catalytic performance of the black phosphorus layer is greatly reduced and most of the black phosphorus is oxidized. Figure 5h shows the current-time curve for Ex-BP/NGS@C. After four months, the current density retention time is still about 6 h, which is similar to the previous test results. There is a partial decrease in its intensity, which is consistent with the small changes in current density observed in Figure 5e.

In order to better evaluate the capability of Ex-BP/NGS@C, we have compiled the recent reported work of black phosphorus materials in OER (Table 1). In the above materials, the sample synthesized in this work Ex-BP/NGS@C has the smallest onset potential of 1.43 V, which is slightly less than 1.44 V of Co/BP. At the same time, compared with the materials mentioned in the table, Ex-BP/NGS@C can have a smaller Tafel slope without adding metal elements that have strong catalytic activity for oxygen evolution reaction.

Table 1. Comparison of OER performance of Ex-BP/NGS@C with other reported samples containing black phosphorus in an alkaline environment.

Sample	Onset Potential (V)	Potential at the Current Density of 10 mA/cm ² (V)	Tafel Slope (mV dec ⁻¹)	Electrolyte	References
Ex-BP/NGS@C	1.43 V vs. RHE	1.55 V vs. RHE	52	1 M KOH.	This work
Few-Layer BP	1.45V vs. RHE	-	88	1 M KOH.	[35]
BP-CNT	1.49 V vs. RHE	1.6 V vs. RHE	72.88	0.1 M KOH.	[36]
BP-Co ₂ P	1.53 V vs. RHE	1.61 V vs. RHE	78	1 M KOH.	[15]
Co/BP	1.44 V vs. RHE	1.54 V vs. RHE	61	1 M KOH.	[36]
Co ₃ O ₄ /N-RGO	1.5 V vs. RHE	1.54 V vs. RHE	67	1 M KOH.	[37]
FPQD	-	1.66 V vs. RHE	49	1 M NaOH.	[38]

By the above results, the excellent electrocatalytic performance of Ex-BP/NGS@C for OER could be due to good exfoliation of Ex-BP and the protection of both NGS and the carbon-coating layer. The carbon coating layer offers strong combination between Ex-BP and NGS in the hybrids, which increased electrical connectivity and maintained the stability of electrode. Better stability of the Ex-BP/NGS@C indicates that the amorphous carbon coating layer plays a key role in the hybrid materials. The combination of NGS and carbon-coating layer can prevent the oxidation of Ex-BP nanosheets. And, the adding of the NGS also plays an important role not only in enhancing the electrical conductivity, but also in facilitating the ion transport, which offers efficient electrochemical reaction kinetics.

4. Conclusions

We have developed a facile method to fabricate a stable BP-based OER catalyst by combining carbon-coating and N-doped graphene nanosheets in a room temperature process. The Ex-BP nanosheets were produced by shearing exfoliation of bulk BP under chemical insertion assistance. The carbon coating layers was obtained by liquid NaK alloy reduction using CO₂ as the carbon source. The coated carbon-coating on Ex-BP nanosheets can avoid structural degradation and keep them stable. The Ex-BP/NGS@C hybrid presents excellent oxygen evolution electrocatalytic performance with an overpotential of 257 mV at 10 mA cm⁻², a small Tafel slope of 41.3 mV dec⁻¹ and high durability under alkaline conditions. Moreover, our work provides a new way to make carbon coatings at room temperature using CO₂ as the carbon source that is green and environmentally friendly and also affords an effective way for the fixation and utilization of CO₂ greenhouse gas. We believe that carbon-coating layers made by this method will open new possibilities for fundamental studies and practical applications.

Supplementary Materials: The following are available online at <http://www.mdpi.com/2079-6412/10/7/695/s1>, Figure S1: TEM image of Ex-BP nanosheets; Figure S2: AFM image of Ex-BP nanosheets; Figure S3: (a) Equipment for synthesizing Ex-BP/NGS@C. (b) Photos of the synthesis process. (c) Image of Ex-BP/NGS@C aqueous dispersion; Figure S4: FTIR spectrum of Ex-BP/NGS@C.

Author Contributions: H.F. conceived and designed experiments. M.Z. and M.F. performed sample characterization and electrochemical studies. H.F., M.Z., W.Z., X.Y., and M.F. were involved in discussions on the design and interpretation of the experiments. H.F. and M.Z. analysed experimental data and wrote the paper. All authors have read and agreed to the published version of the manuscript.

Funding: This research was funded by the National Natural Science Foundation of China (No. 21501172) and the Key R & D programs in Shandong (No. 2018GGX102038), the Applied Basic Research Program Project of Qingdao (No. 17-1-1-69-jch).

Acknowledgments: We thank the support from the World-Class University and Discipline Program of Shandong Province and the Taishan Scholars Advantageous and Distinctive Discipline Program of Shandong Province, China.

Conflicts of Interest: The authors declare no conflict of interest.

References

1. Choi, J.W.; Aurbach, D. Promise and reality of post-lithium-ion batteries with high energy densities. *Nat. Rev. Mater.* **2016**, *1*. [[CrossRef](#)]
2. Wang, H.; Yu, D.; Kuang, C.; Cheng, L.; Li, W.; Feng, X.; Zhang, Z.; Zhang, X.; Zhang, Y. Alkali metal anodes for rechargeable batteries. *Chem* **2019**, *5*, 313–338. [[CrossRef](#)]
3. Liu, D.; Li, X.; Chen, S.; Yan, H.; Wang, C.; Wu, C.; Haleem, Y.A.; Duan, S.; Lu, J.; Ge, B.; et al. Atomically dispersed platinum supported on curved carbon supports for efficient electrocatalytic hydrogen evolution. *Nat. Energy* **2019**, *4*, 512–518. [[CrossRef](#)]
4. Zhang, J.; Ren, M.; Wang, L.; Li, Y.; Yakobson, B.I.; Tour, J.M. Oxidized laser-induced graphene for efficient oxygen electrocatalysis. *Adv. Mater.* **2018**, *30*, 1707319. [[CrossRef](#)] [[PubMed](#)]
5. Kim, M.; Lee, B.; Ju, H.; Lee, S.W.; Kim, J. Reducing the barrier energy of self-reconstruction for anchored cobalt nanoparticles as highly active oxygen evolution electrocatalyst. *Adv. Mater.* **2019**, *31*, 1901977. [[CrossRef](#)] [[PubMed](#)]
6. Wang, M.; Lin, M.; Li, J.; Huang, L.; Zhuang, Z.; Lin, C.; Zhou, L.; Mai, L. Metal-organic framework derived carbon-confined Ni₂P nanocrystals supported on graphene for an efficient oxygen evolution reaction. *Chem. Commun.* **2017**, *53*, 8372–8375. [[CrossRef](#)] [[PubMed](#)]
7. Seitz, L.C.; Dickens, C.F.; Nishio, K.; Hikita, Y.; Montoya, J.; Doyle, A.; Kirk, C.; Vojvodic, A.; Hwang, H.Y.; Nørskov, J.K.; et al. A highly active and stable IrOx/SrIrO₃ catalyst for the oxygen evolution reaction. *Science* **2016**, *353*, 1011–1014. [[CrossRef](#)]
8. Li, Z.; Zhang, X.; Cheng, H.; Liu, J.; Shao, M.; Wei, M.; Evans, D.G.; Zhang, H.; Duan, X. Confined synthesis of 2D nanostructured materials toward electrocatalysis. *Adv. Energy Mater.* **2020**, *10*, 1900486. [[CrossRef](#)]
9. Chen, Y.C.; Lu, A.Y.; Lu, P.; Yang, X.; Jiang, C.M.; Mariano, M.; Kaehr, B.; Lin, O.; Taylor, A.; Sharp, I.D.; et al. Structurally deformed MoS₂ for electrochemically stable, thermally resistant, and highly efficient hydrogen evolution reaction. *Adv. Mater.* **2017**, *29*, 1703863. [[CrossRef](#)]
10. García de Arquer, F.P.; Bushuyev, O.S.; De Luna, P.; Dinh, C.T.; Seifitokaldani, A.; Saidaminov, M.I.; Tan, C.S.; Quan, L.N.; Proppe, A.; Kibria, M.G.; et al. 2D Metal oxyhalide-derived catalysts for efficient CO₂ electroreduction. *Adv. Mater.* **2018**, *30*, 6–11. [[CrossRef](#)]
11. Rubio, R.; Santander, J.; Fonseca, L.; Sabate, N.; Gracia, I.; Cane, C.; Udina, S.; Marco, S. Non-selective NDIR array for gas detection. *Sens. Actuators B Chem.* **2007**, *127*, 69–73. [[CrossRef](#)]
12. Yuan, Z.; Li, J.; Yang, M.; Fang, Z.; Jian, J.; Yu, D.; Chen, X.; Dai, L. Ultrathin black phosphorus-on-nitrogen doped graphene for efficient overall water splitting: Dual modulation roles of directional interfacial charge transfer. *J. Am. Chem. Soc.* **2019**, *141*, 4972–4979. [[CrossRef](#)] [[PubMed](#)]
13. Zhang, K.; Jin, B.; Park, C.; Cho, Y.; Song, X.; Shi, X.; Zhang, S.; Kim, W.; Zeng, H.; Park, J.H. Black phosphorene as a hole extraction layer boosting solar water splitting of oxygen evolution catalysts. *Nat. Commun.* **2019**, *10*, 2001. [[CrossRef](#)] [[PubMed](#)]
14. Shi, F.; Geng, Z.; Huang, K.; Liang, Q.; Zhang, Y.; Sun, Y.; Cao, J.; Feng, S. Cobalt nanoparticles/black phosphorus nanosheets: An efficient catalyst for electrochemical oxygen evolution. *Adv. Sci.* **2018**, *5*. [[CrossRef](#)]
15. Wang, J.; Liu, D.; Huang, H.; Yang, N.; Yu, B.; Wen, M.; Wang, X.; Chu, P.K.; Yu, X.F. In-plane black phosphorus/dicobalt phosphide heterostructure for efficient electrocatalysis. *Angew. Chem. Int. Ed.* **2018**, *57*, 2600–2604. [[CrossRef](#)]
16. Brent, J.R.; Ganguli, A.K.; Kumar, V.; Lewis, D.J.; McNaughtner, P.D.; O'Brien, P.; Sabherwal, P.; Tedstone, A.A. On the stability of surfactant-stabilised few-layer black phosphorus in aqueous media. *RSC Adv.* **2016**, *6*, 86955–86958. [[CrossRef](#)]

17. Tan, S.J.R.; Abdelwahab, I.; Chu, L.; Poh, S.M.; Liu, Y.; Lu, J.; Chen, W.; Loh, K.P. Quasi-monolayer black phosphorus with high mobility and air stability. *Adv. Mater.* **2018**, *30*, 1704619. [[CrossRef](#)]
18. Zhang, Y.; Dong, N.; Tao, H.; Yan, C.; Huang, J.; Liu, T.; Robertson, A.W.; Texter, J.; Wang, J.; Sun, Z. Exfoliation of 2D Black Phosphorus for Device Fabrication. *Chem. Mater.* **2017**, *29*, 6445–6456. [[CrossRef](#)]
19. Edmonds, M.T.; Tadich, A.; Carvalho, A.; Ziletti, A.; O'Donnell, K.M.; Koenig, S.P.; Coker, D.F.; Özyilmaz, B.; Neto, A.H.C.; Fuhrer, M.S. Creating a stable oxide at the surface of black phosphorus. *ACS Appl. Mater. Interfaces* **2015**, *7*, 14557–14562. [[CrossRef](#)]
20. Gusmão, R.; Sofer, Z.; Pumera, M. Functional protection of exfoliated black phosphorus by noncovalent modification with anthraquinone. *ACS Nano* **2018**, *12*, 5666–5673. [[CrossRef](#)]
21. Abate, Y.; Akinwande, D.; Gamage, S.; Wang, H.; Snure, M.; Poudel, N.; Cronin, S.B. Recent progress on stability and passivation of black phosphorus. *Adv. Mater.* **2018**, *30*, 1704749. [[CrossRef](#)] [[PubMed](#)]
22. Walia, S.; Balendhran, S.; Ahmed, T.; Singh, M.; El-Badawi, C.; Brennan, M.D.; Weerathunge, P.; Karim, M.N.; Rahman, F.; Russell, A.; et al. Ambient protection of few-layer black phosphorus via sequestration of reactive oxygen species. *Adv. Mater.* **2017**, *29*, 1700152. [[CrossRef](#)] [[PubMed](#)]
23. Qiu, S.; Zhou, Y.; Zhou, X.; Zhang, T.; Wang, C.; Yuen, R.K.K.; Hu, W.; Hu, Y. Air-stable polyphosphazene-functionalized few-layer black phosphorene for flame retardancy of epoxy resins. *Small* **2019**, *15*, 1805175. [[CrossRef](#)] [[PubMed](#)]
24. Feng, M.; Zhang, M.; Zhang, H.; Liu, X.; Feng, H. Room-temperature carbon coating on MoS₂/graphene hybrids with carbon dioxide for enhanced sodium storage. *Carbon* **2019**, *153*, 217–224. [[CrossRef](#)]
25. Wu, X.; Wang, Z.; Yu, M.; Xiu, L.; Qiu, J. Stabilizing the mxenes by carbon nanoplating for developing hierarchical nanohybrids with efficient lithium storage and hydrogen evolution capability. *Adv. Mater.* **2017**, *29*. [[CrossRef](#)]
26. Park, J.E.; Jang, Y.S.; Bae, T.S.; Lee, M.H. Multi-walled carbon nanotube coating on alkali treated TiO₂ nanotubes surface for improvement of biocompatibility. *Coatings* **2018**, *8*, 159. [[CrossRef](#)]
27. Feng, H.; Hu, Z.; Liu, X. Facile and efficient exfoliation of inorganic layered materials using liquid alkali metal alloys. *Chem. Commun.* **2015**, *51*, 10961–10964. [[CrossRef](#)]
28. Feng, H.; Cheng, R.; Zhao, X.; Duan, X.; Li, J. A low-temperature method to produce highly reduced graphene oxide. *Nat. Commun.* **2013**, *4*, 1539. [[CrossRef](#)]
29. Brent, J.R.; Savjani, N.; Lewis, E.A.; Haigh, S.J.; Lewis, D.J.; O'Brien, P. Production of few-layer phosphorene by liquid exfoliation of black phosphorus. *Chem. Commun.* **2014**, *50*, 13338–13341. [[CrossRef](#)]
30. Sun, J.; Lee, H.W.; Pasta, M.; Yuan, H.; Zheng, G.; Sun, Y.; Li, Y.; Cui, Y. A phosphorene-graphene hybrid material as a high-capacity anode for sodium-ion batteries. *Nat. Nanotechnol.* **2015**, *10*, 980–985. [[CrossRef](#)]
31. Favron, A.; Gauffrès, E.; Fossard, F.; Phaneuf-Laheureux, A.L.; Tang, N.Y.W.; Lévesque, P.L.; Loiseau, A.; Leonelli, R.; Francoeur, S.; Martel, R. Photooxidation and quantum confinement effects in exfoliated black phosphorus. *Nat. Mater.* **2015**, *14*, 826–832. [[CrossRef](#)]
32. Kuntz, K.L.; Wells, R.A.; Hu, J.; Yang, T.; Dong, B.; Guo, H.; Woomer, A.H.; Druffel, D.L.; Alabanza, A.; Tománek, D.; et al. Control of surface and edge oxidation on phosphorene. *ACS Appl. Mater. Interfaces* **2017**, *9*, 9126–9135. [[CrossRef](#)] [[PubMed](#)]
33. Song, T.; Chen, H.; Xu, Q.; Liu, H.; Wang, Y.-G.; Xia, Y. Black phosphorus stabilizing Na₂Ti₃O₇/C each other with an improved electrochemical property for sodium-ion storage. *ACS Appl. Mater. Interfaces* **2018**, *10*, 37163–37171. [[CrossRef](#)]
34. Sun, J.; Zheng, G.; Lee, H.W.; Liu, N.; Wang, H.; Yao, H.; Yang, W.; Cui, Y. Formation of stable phosphorus-carbon bond for enhanced performance in black phosphorus nanoparticle-graphite composite battery anodes. *Nano Lett.* **2014**, *14*, 4573–4580. [[CrossRef](#)] [[PubMed](#)]
35. Ren, X.; Zhou, J.; Qi, X.; Liu, Y.; Huang, Z.; Li, Z.; Ge, Y.; Dhanabalan, S.C.; Ponraj, J.S.; Wang, S.; et al. Few-layer black phosphorus nanosheets as electrocatalysts for highly efficient oxygen evolution reaction. *Adv. Energy Mater.* **2017**, *7*, 1700396. [[CrossRef](#)]
36. Jiang, Q.; Xu, L.; Chen, N.; Zhang, H.; Dai, L.; Wang, S. Facile synthesis of black phosphorus: An efficient electrocatalyst for the oxygen evolving reaction. *Angew. Chem. Int. Ed.* **2016**, *55*, 13849–13853. [[CrossRef](#)]

37. Liang, Y.; Li, Y.; Wang, H.; Zhou, J.; Wang, J.; Regier, T.; Dai, H. Co₃O₄ nanocrystals on graphene as a synergistic catalyst for oxygen reduction reaction. *Nat. Mater.* **2011**, *10*, 780–786. [[CrossRef](#)]
38. Prasannachandran, R.; Vineesh, T.V.; Anil, A.; Krishna, B.M.; Shaijumon, M.M. Functionalized phosphorene quantum dots as efficient electrocatalyst for oxygen evolution reaction. *ACS Nano* **2018**, *12*, 11511–11519. [[CrossRef](#)]



© 2020 by the authors. Licensee MDPI, Basel, Switzerland. This article is an open access article distributed under the terms and conditions of the Creative Commons Attribution (CC BY) license (<http://creativecommons.org/licenses/by/4.0/>).